Electronic Supplementary Information for

Ordering kinetics of lamella-forming block copolymers under guidance of various external fields studied by dynamic self-consistent field theory

Xiaomin Wan, Tong Gao, Liangshun Zhang, and Jiaping Lin**

Shanghai Key Laboratory of Advanced Polymeric Materials, State Key Laboratory of Bioreactor Engineering, Key Laboratory for Ultrafine Materials of Ministry of Education, School of Materials Science and Engineering, East China University of Science and Technology, Shanghai 200237, China.

*Corresponding Author E-mail: zhangls@ecust.edu.cn (Zhang L.); jlin@ecust.edu.cn (Lin J.)

Contents

Part A: Defect analysis of lamellar nanostructures

Figure S1 presents visual outline of defect analysis for the lamellar nanostructures. In brief, the configurations of local density fields of A and B blocks are first thresholded to create binary images suitable for subsequent analysis (Figure S1b). Then, both A- and B-rich lamellae identified in the binary images are isolated and converted into topological skeletons via the thinning algorithm (Figure S1c),[S1] which maintain the connectivity of original configurations of density fields. Lastly, on the basis of Kléman's ideas,[S2] the junctions and the terminal points of skeletons are utilized to identify the lamellar defects in two-dimensional space (Figure S1d). In the block copolymer systems, frequently encountered defects are the dislocations (pairs of adjacent junction and terminal point) and the disclinations (either terminal points or junctions), which are highlighted by the dashed circles in Figure S1d. Herein, we do not distinguish the dislocations and disclinations within the samples, and only the total number n_d of terminal points and junctions in both the A- and B-rich lamellae is collected from the skeleton analysis.[S3] The areal defect density abbreviated as *DD* is defined by $DD \equiv n_d/2\mathrm{A}$, where A is the area of entire samples.

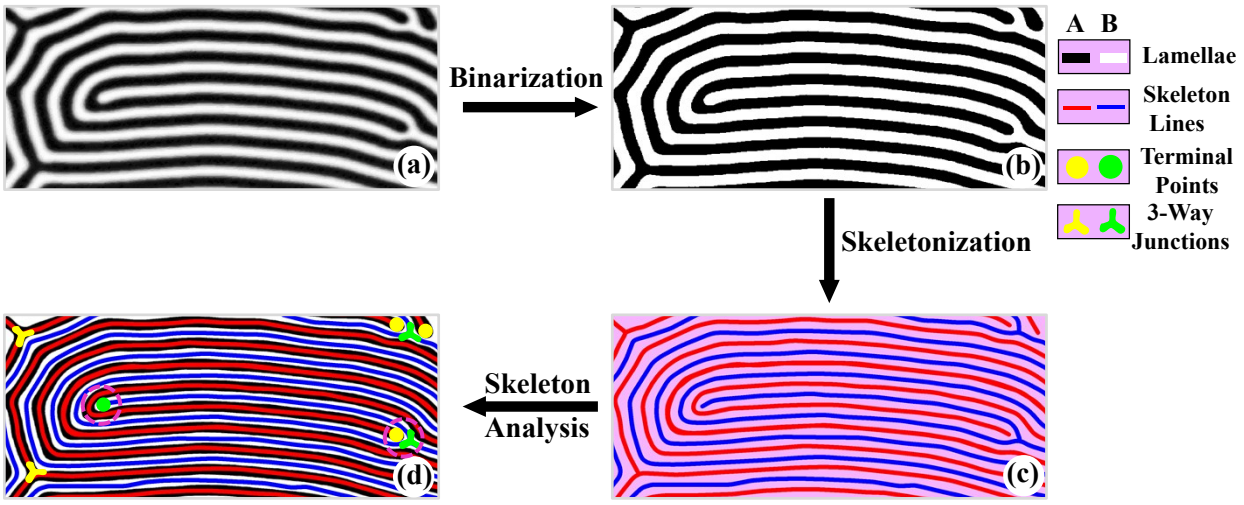

Figure S1. Visual outline of defect identification for the lamellar nanostructures in two-dimensional space. (a) Raw image of self-assembled nanostructures obtained from the simulations. (b) Thresholding self-assembled configuration to generate a binary image. The black (white) regions indicate the A-rich (B-rich) lamellae. (c) Skeletonization of the lamellae. The red and blue lines correspond to the skeletonized lines of A- and B-rich lamellae, respectively. (d) Skeleton analysis for the defects. The skeleton lines are overlaid on the original image. The solid circles and 3-connected branches represent the terminal points and 3-way junctions of skeleton lines, respectively. The dashed circles highlight the disclination (terminal point) and the dislocation (pair of 3-way junction and terminal point).

Part B: Effect of Flory-Huggins interaction parameter

The Flory-Huggins interaction parameter $(\chi N)_{min}$ in the α region critically impacts the self-assembly behaviors of block copolymers. Figure S2 presents the morphological evolution of self-assembled nanostructures in the presence of zone annealing at $(\chi N)_{min}$=9.0, 12.0 and 14.0. For the symmetric block copolymers, the Flory-Huggins interaction parameter of order-disorder transition is $(\chi N)_{ODT}$=10.5. As $(\chi N)_{min}<(\chi N)_{ODT}$, the phase-separated domains in the α region transit to a disordered phase, which is demonstrated by the profiles of local density fields of A and B blocks in the inset of Figure S2a. As the block copolymers are moved out the α region, the existing lamellae serve as 'chemical template' to direct the self-assembly of polymeric fluids. Thus, the perfect ordering of lamellar nanostructures with perpendicular orientation is achieved in the entire sample (Figure S2a). In the weak segregation limit (*e.g.*, $(\chi N)_{min}$=12.0) of block copolymers, the ordering of self-assembled nanodomains occurs via the defect annihilation, resulting in formation of highly ordered nanostructures (Figure S2b). While $(\chi N)_{min}$ has a value of 14.0, the ordering degree of lamellar nanostructures has an improvement, but the large lamellar grains with different orientations are maintained in the samples owing to higher energy barrier of structural rearrangement (Figure S2c).

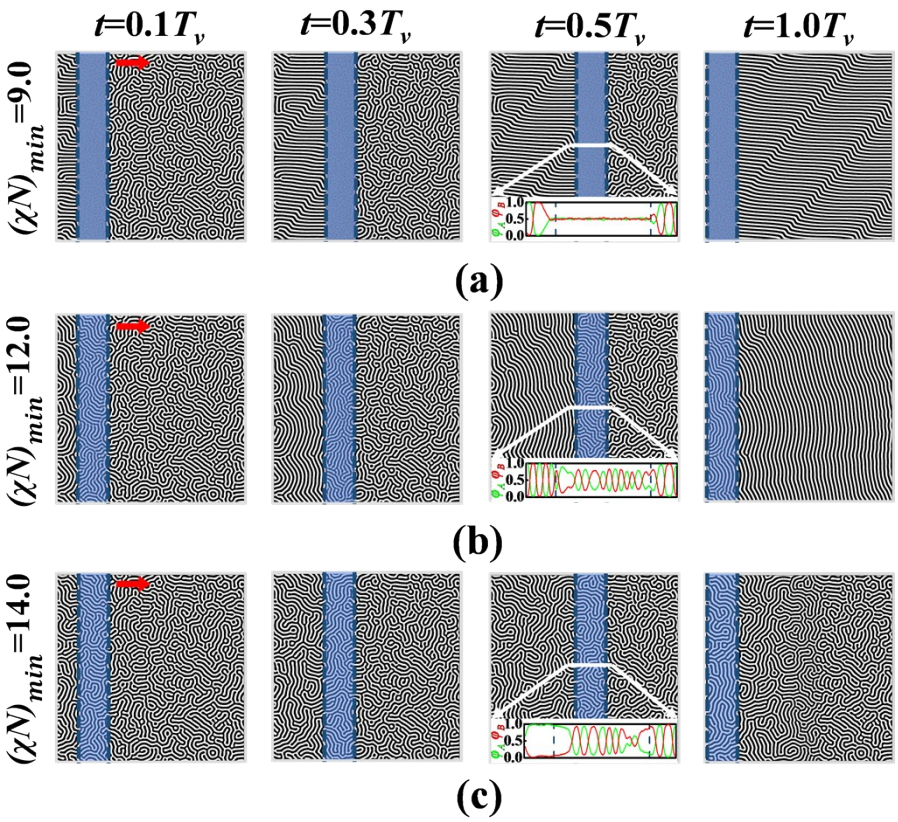

Figure S2. Effect of Flory-Huggins interaction parameter $(\chi N)_{min}$ on ordering behaviors of block copolymers subjected to the zone annealing. (a) Structural evolution of block copolymers subjected to the zone annealing with $(\chi N)_{min}$=9.0 in the α region, (b) structural evolution of block copolymers for the case of $(\chi N)_{min}$=12.0 and (c) structural evolution of block copolymers for the case of $(\chi N)_{min}$=14.0. The zone width and the sweep velocity are fixed at w=32.0R_g and v=0.30$\tilde{v}$, respectively. The period T_v of zone annealing is 640.0τ. Insets are the profiles of local density fields of A and B blocks across the solid lines.

Part C: Morphological evolution of undulated lamellae

The undulated lamellae usually observed in the α region of zone annealing are able to further evolve into the low internal-stress configurations, which are illustrated in Figure S3. Two types of simulations are performed. One is that the Flory-Huggins interaction parameters in the entire sample are set as $(\chi N)_{max}=(\chi N)_{min}=20.0$. As shown in Figure S3a, a long relaxation relieves the lamellar modulation and the undulated lamellae finally recover the straight shapes. The other is that the α region is stationary, corresponding to the case of $v=0$. In the α region, the block copolymers have sufficient time to reassemble, leading to reproductions of defects at the annealed zone with $(\chi N)_{min}=12.0$ (Figure S3b).

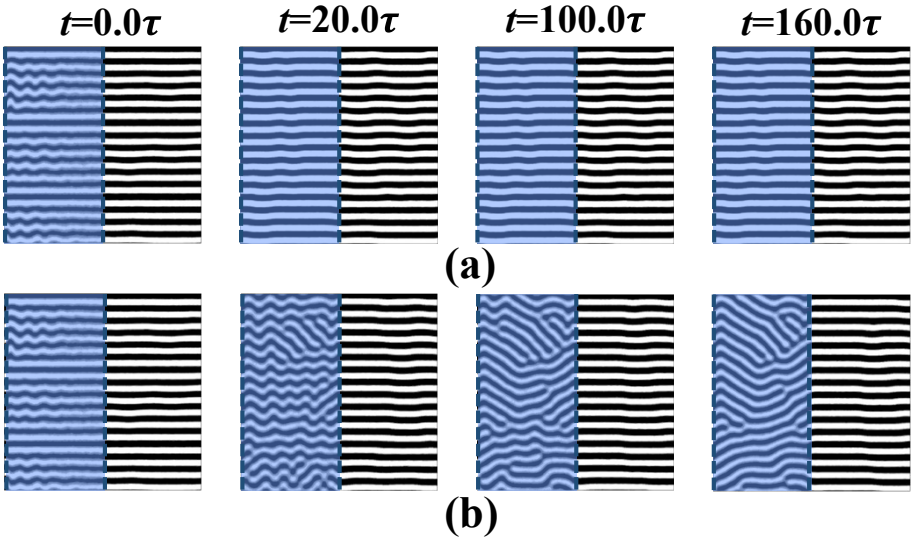

Figure S3. Morphological evolution of undulated lamellae in response to the change of computational parameters. (a) Flory-Huggins interaction parameters $(\chi N)_{max}=(\chi N)_{min}=20.0$ in the entire sample. (b) Stationary α region in the simulations of dynamic self-consistent field theory. The Flory-Huggins interaction parameter in the α region is set as $(\chi N)_{min}=12.0$. The times are indicated on the top of image (a). The snapshots are extracted from the identical region of an extremely large simulation box.

Part D: Zone-annealed block copolymers at extremely slow sweep velocity

As the sweep velocity is extremely slow (v=0.075$\tilde{v}$), the zone-annealed block copolymers in the α region have enough time to fully rearrange (Figure S4). To accommodate the lamellae with a smaller period, the defects of lamellar nanostructures are reproduced in the α region under the quasistatic condition.

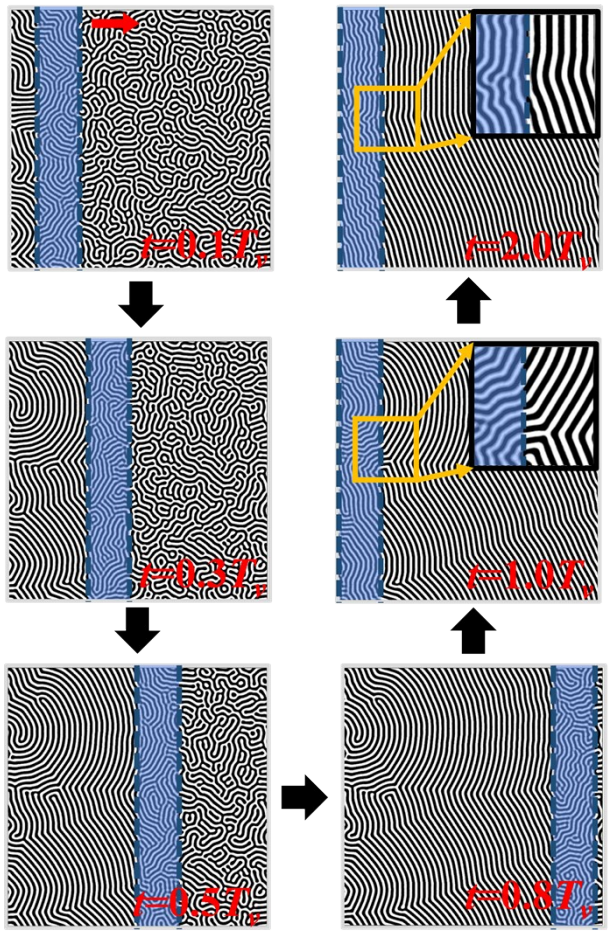

Figure S4. Structural evolution of block copolymers subjected to the zone annealing under the zone width w=32.0R_g and the sweep velocity v=0.075$\tilde{v}$. The characteristic time T_v of zone annealing is T_v=2560.0τ. The time normalized by T_v is shown in each snapshot. Insets show a close-up of the block copolymer nanostructures enclosed in the boxes.

Part E: Dislocation dipoles in the presence of zone annealing

DSCFT simulations provide directly insight into the process of defect annihilation for the block copolymers subjected to the space- and time-dependent field. A typical procedure of defect annihilation is illustrated in Figure S5. A portion of the lamellar configurations are extracted from the profiles of local density fields of A and B blocks, and the relative evolution time Δt is shown in each snapshot. Pairs of dislocations with 1/2 and -1/2 cores are the frequently encountered defects in the β region with higher Flory-Huggins interaction parameter $(\chi N)_{max}$=20.0 (relative time Δt=0.0τ in Figure S5). As the α region with lower Flory-Huggins interaction parameter $(\chi N)_{min}$=12.0 approaches the defects, the left dislocation with +1/2 B core is converted into the dislocation with +1/2 A core, apparently due to one end of the dislocated lamella moving left to bridge its neighbor (Δt=27.0τ). Subsequently, the continuous movement of annealed zone triggers the bridge formation of the right dislocation in a similar manner (Δt=43.0τ). Eventually, two dislocated lamellae fully covered by the α region are brought together (Δt=50.0τ), connected (Δt=57.0τ) and straightened (Δt=80.0τ).

The parameter settings of annealed zone remarkably affect the defect annhilation of lamellar nanostructures, which is illustrated in Figure S6. As the Flory-Huggins interaction paramter $(\chi N)_{min}$ in the α region is increased to 18.0, the dislocation dipoles are preserved in the samples due to the higher energy barrrier of defect annihilation (Figure S6a). When the residence time is too short (corresponding to the fast sweep velocity), the dislocation dipoles are not affected by the mobile α region (Figure S6b). As the sweep velocity becomes slow, the imperfections emerge in the annealed zone (Figure S6c).

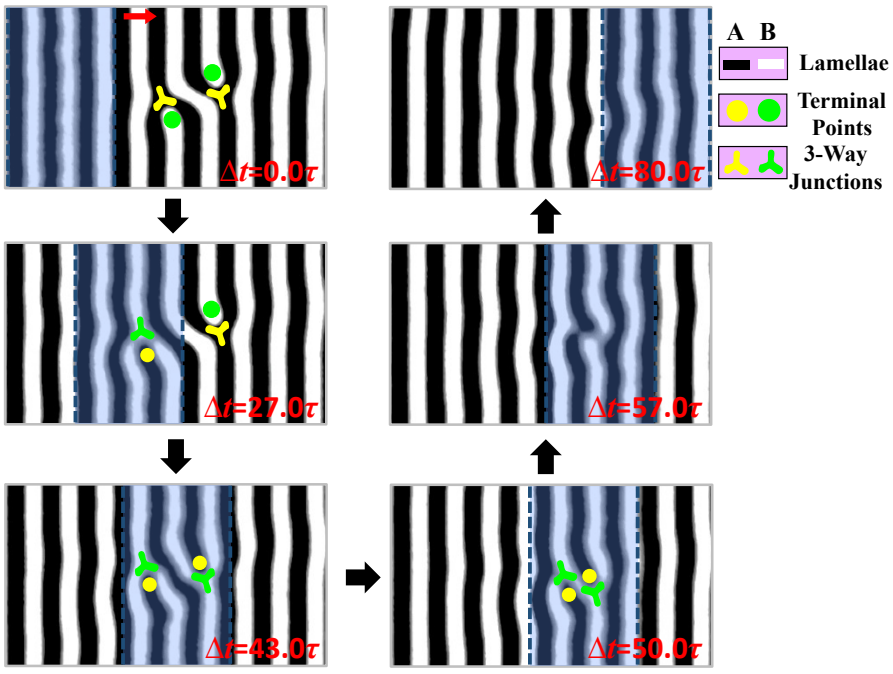

Figure S5. Typical procedure of defect annihilation for dislocation dipoles in the presence of zone annealing. The snapshots are extracted from identical region of a much large simulation box. The evolution time is shown in each snapshot. The Flory-Huggins interaction parameter in the α region is $(\chi N)_{min}$=12.0. The zone width and sweep velocity have values of w=12.0R_g and v =0.30$\tilde{v}$, respectively. The solid circles and 3-connected branches represent the 1/2 and -1/2 cores of defects, respectively.

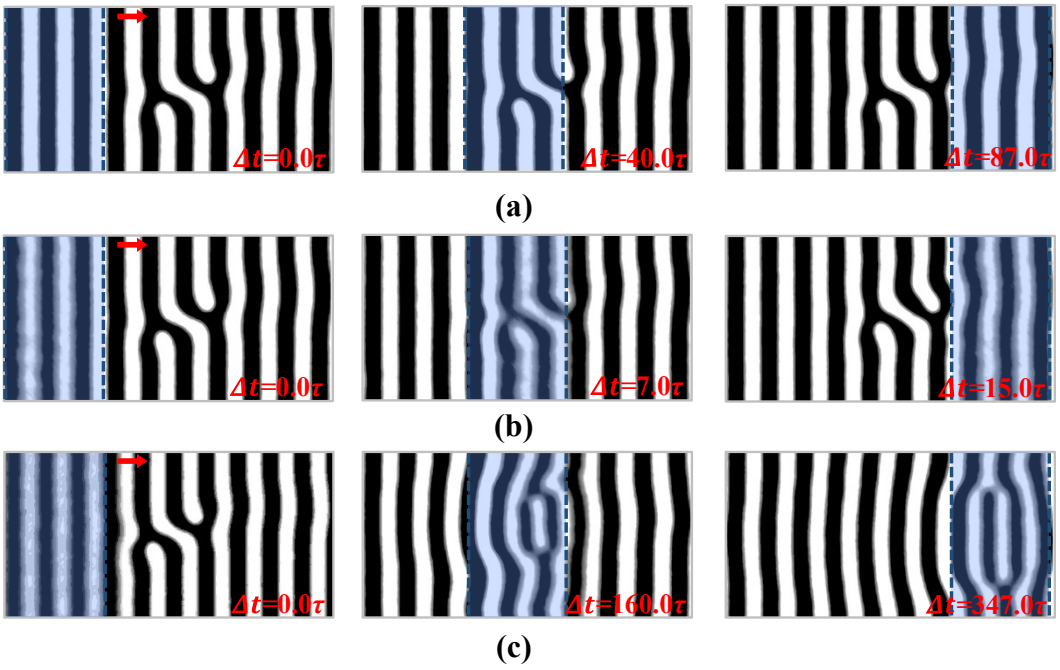

Figure S6. Sequential snapshots of structural evolution of dislocation dipoles in the presence of zone annealing with various combinations of Flory-Huggins interaction parameter $(\chi N)_{min}$ and the sweep velocity v. The key parameters of zone annealing are the same as those in Figure S5 except one parameter. (a) The Flory-Huggins interaction parameter is changed from $(\chi N)_{min}$=12.0 to $(\chi N)_{min}$= 18.0. (b) The sweep velocity is varied from v=0.30$\tilde{v}$ to v=0.90$\tilde{v}$. (c) The sweep velocity is varied from v=0.30$\tilde{v}$ to v=0.075$\tilde{v}$.

Part F: Effect of initial configurations

Initial configurations of computer simulations strongly impact the pathway of ordering, but weakly affect the final self-assembled nanostructures for the integrated chemical templates/zone annealing method. As metastable states from the zone annealing simulations are chosen as initial configurations, there is an increase of defect density in the samples due to the formation of grain boundary around the guiding stripes (at time t=0.15T_v of Figure S7a). Subsequently, the zone annealing effectively removes the defects in the soft confinement environment. Eventually, such polycrystalline nanostructures with multiple orientations evolve into the large-area ordered nanopatterns with registered orientations (Figure S7a). For the simulations of homogeneous states, lots of defects are formed between the guiding stripes at the initial stage, and are quickly eliminated in the first and second passages of zone annealing. In the fourth passage of zone annealing, the block copolymers are guided to self-assemble into the defect-free lamellae precisely aligned along the x direction (Figure S7b).

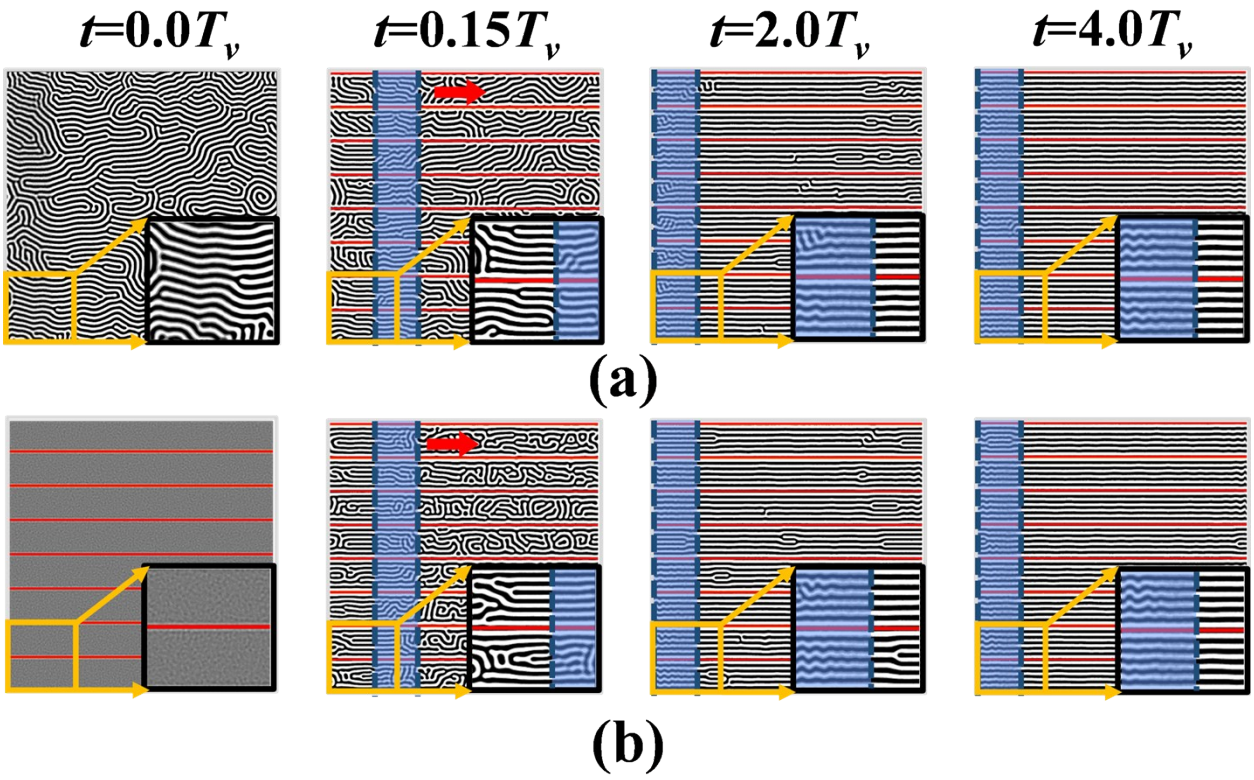

Figure S7. Morphological evolution of self-assembled nanostructures in the presence of dual fields. The initial configurations of simulations are chosen from (a) the metastable states of zone annealing simulations and (b) the homogenous states. The normalized times are shown on the top of images. Insets show a close-up of the block copolymer nanostructures enclosed in the boxes. The period of guiding stripes is set as L_s=6L_0. The zone width and the sweep velocity are fixed at w=32.0R_g and v=0.75$\tilde{v}$, respectively.

Part G. Effect of tilt angles

To evaluate the robustness of integrated method for the long-range ordered nanostructures, we implement a series of simulations of block copolymers in the presence of dual field with various tilt angles Φ, which is schemed in the inset of Figure S8a. The corresponding morphological evolution of nanostructures and the temporal evolution of defect density are depicted in Figures S8 and S9, respectively. Like the case of Φ=0 (Figure S7b), the block copolymers guided by the dual field with various tilt angles self-assemble into the defective lamellae at the initial stage. Subsequently, such defects are quickly eliminated by the zone annealing. Eventually, the defect-free lamellae aligned along the direction of guiding stripes are achieved in the simulations (Figure S8). As shown in Figure S9, the temporal evolutions of defect density under various tilt angles confirm this tendency of ordering process of block copolymers. Given these observations, one can conclude that the tilt angles between the permanent and dynamic fields have a weak influence on the ordering degree and kinetics of self-assembled nanostructures, suggesting the robustness of dual-field method.

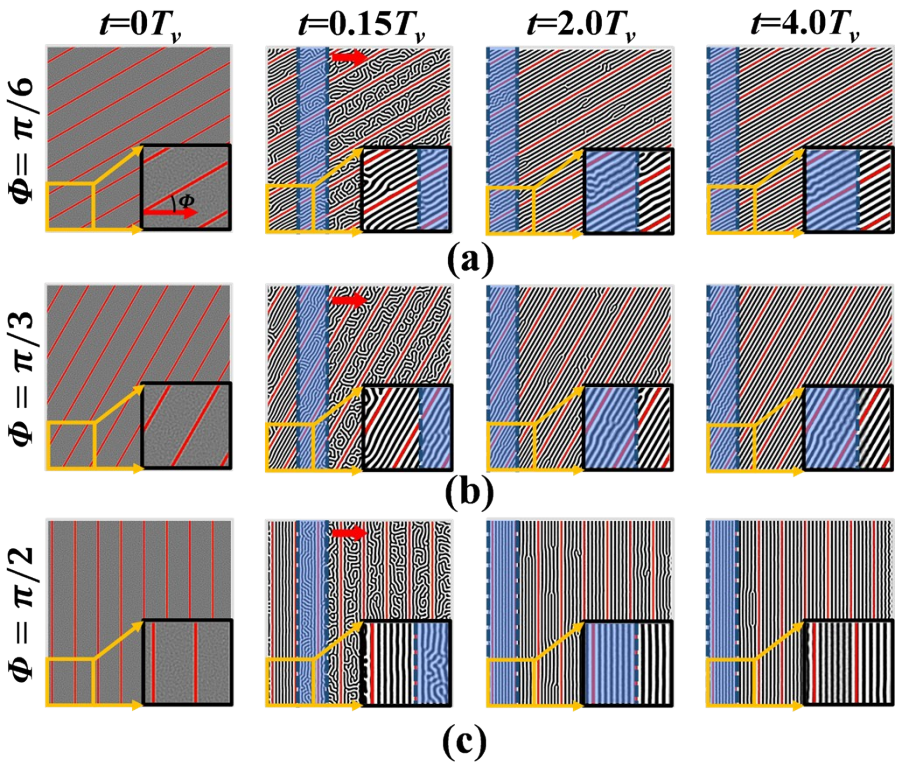

Figure S8. Morphological evolution of self-assembled nanostructures in the presence of dual field under various tilt angles Φ between the direction of guiding stripes and the moving direction of α region. (a) $\Phi=\pi/6$, (b) $\Phi=\pi/3$ and (c) $\Phi=\pi/2$. Inset of the image (a) shows the definition of tilt angle. The case of $\Phi=0$ is shown in Figure S7b. The initial configurations of simulations are homogenous states. The parameter settings and representations are the same as Figure S7.

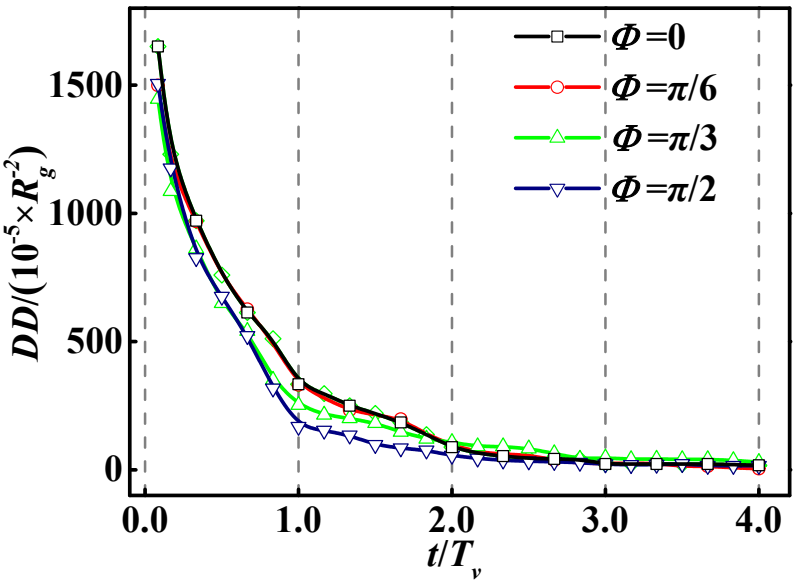

Figure S9. Temporal evolution of defect density of self-assembled nanostructures obtained from the simulations of integrated method under various tilt angles Φ. The parameter settings are the same as Figure S7.

Part H: Block copolymers guided by extremely sparse stripes

Figure S10 shows the structural evolution and the lamellar orientation distributions of block copolymers subjected to the dual fields at the period L_s=12L_0 of guiding stripes for various sweep velocities. For the slow sweep velocity v=0.38$\tilde{v}$, the block copolymers guided by the extremely sparse stripes successfully self-assemble into the long-range ordered lamellae with precisely registered orientation (Figure S10a). As the α region is shifted fast, the grain boundaries are still observed at the annealing time t=6.0T_v (Figure S10b).

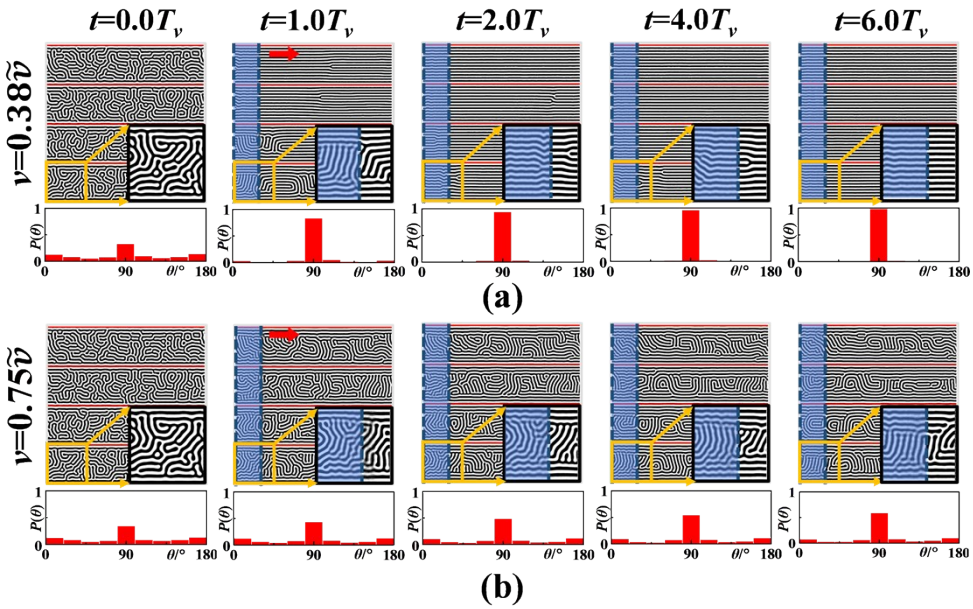

Figure S10. (Top panels) Morphological evolution and (bottom panels) local orientation distribution of self-assembled nanostructures for integration of chemical templates with extremely sparse guiding stripes L_s=12L_0 and zone annealing with sweep velocities (a) v=0.38$\tilde{v}$ and (b) v=0.75$\tilde{v}$. The initial configurations are chosen from the metastable states of chemical template simulations. The normalized times are shown on the top of images. Insets show a close-up of the block copolymer nanostructures enclosed in the boxes.

REFERENCES

(S1) T. Y. Zhang and C. Y. Suen, *Commun. ACM,* 1984, **27**, 236-239.

(S2) M. Kléman, *Points, lines, and walls: in liquid crystals, magnetic systems, and various ordered media*, John Wiley & Sons, 1983.

(S3) J. N. Murphy, K. D. Harris and J. M. Buriak, *PLoS ONE,* 2015, **10**, e0133088.